RSC Advances

ROYAL SOCIETY OF CHEMISTRY

PAPER

View Article Online
View Journal | View Issue

Check for updates

Cite this: *RSC Adv.*, 2021, **11**, 34779

# A novel 3D terbium metal–organic framework as a heterogeneous Lewis acid catalyst for the cyanosilylation of aldehyde†

Yuqian Liu, Peiran Zhao, Chunying Duan and Cheng He*

Received 31st August 2021
Accepted 14th October 2021

DOI: 10.1039/d1ra06533e

rsc.li/rsc-advances

A novel 3D lanthanide(III) metal–organic framework (MOF) (namely Tb-MOF), was synthesized by self-assembly from Tb(III) ion nitrate and the rigid organic ligand $H_2$sbdc ($H_2$sbdc = 5,5-dioxo-5*H*-dibenzo[*b*,*d*]thiophene-3,7-dicarboxylic acid), and could work as an efficient heterogeneous catalyst for the cyanosilylation of aromatic aldehydes at room temperature. The obtained Tb-MOF has been characterized and analysed in detail by single crystal X-ray diffraction, powder X-ray diffraction, thermogravimetric analysis and so on. The pores of Tb-MOF provided a microenvironment that was beneficial for the substrates to be close to the Lewis acid catalytic sites. The IR spectrogram and the fluorescence titration proved that the substrates could be activated inside the channel of Tb-MOF. The heterogeneous Tb-MOF catalyst with fine catalytic efficiency exhibited a high TON (TON = 460), and could be recycled at least three times without significantly reducing its activity.

## Introduction

Two- or three-dimensional porous metal–organic frameworks (MOFs) are an important kind of functional materials, which have an inherent advantage of being readily self-assembled *via* suitable organic linkers and inorganic metal ions/clusters.[1] Due to the unlimited coordinated bonds through the metal ions/clusters and the organic linkers, they usually appear as infinite multiple dimension networks, which endow the MOFs with diversified structures and functional applications.[2] Meanwhile they usually have high porosity, large surface area and considerable capacity,[3] which offer a wide range of potential applications in gas storage,[4] gas capture,[5] separation,[6] chemical catalysis,[7] luminescence,[8] magnetism,[9] drug delivery,[10] and so on.

One special type of MOF, the lanthanide MOFs (Ln-MOFs),[11] have attracted extensive attention. Firstly, Ln-MOFs have unique luminescence properties[12] such as linear emission, high color purity, long fluorescence lifetime and so on. Secondly, the high coordination numbers and the flexible coordination geometries endow the Ln-MOFs with abundant topological structures.[13] In addition, the organic linkers can be designed and selected to synthesize MOFs, which can be used as target materials.[14] Thirdly, inside the channels of the MOFs, it contains functional sites such as open metal sites, hydrogen bonding sites and organic coordinate sites, which are highly ordered.[15] Some of the Ln-MOFs are stable and even more stable than their transition-metal-based analogues,[16] which are easy to activate the substrates without its framework collapse.[17] In addition, Ln-MOFs as attractive Lewis acid catalysts have well-proportioned Lewis acid sites within its pores/channels which afford a platform to activate the substrates and make the catalyst reaction continue.[18] Compared to the homogeneous catalysts, the heterogeneous Ln-MOFs can provide uniformly dispersed microenvironment, which is beneficial for the substrates to be close to the functional sites and easy to be separated.[19] Compared to the other heterogenous materials such as zeolites,[20] which have no organic moiety and are generally inactive for reactions in water, the Ln-MOFs can be well designed and tuned.[21]

On the other hand, cyanohydrins are very important for chemistry, which could be widely used for starting materials for the synthesis of many kinds of pivotal intermediates in chemistry, such as α-amino acids, β-amino alcohols, α-hydroxy acids, α-hydroxy ketones, and so on.[22] The product of cyanosilylation of aldehydes with cyanides, such as trimethylsilyl cyanide ($Me_3SiCN$ or TMSCN), which allows the cyanohydrins to be prepared as the corresponding trimethylsilyl ether, could be readily converted into cyanohydrins.[23] As a result, cyanosilylation between aldehydes and $Me_3SiCN$ has attracted a lot of attention from the scientists in the past few years.

Thermally stable MOFs (for example MIL-47 (V), MIL-53 (Al), MIL-101 (Cr), and UiO-66 (Zr)) have been used for catalyzing the cyanosilylation based on their Lewis acid sites.[24] In this paper, the luminescent lanthanide ion Tb(III) was selected to assemble

---

State Key Laboratory of Fine Chemicals, Dalian University of Technology, Dalian, 116024, P. R. China. E-mail: hecheng@dlut.edu.cn

† Electronic supplementary information (ESI) available: Experimental and catalysis details, characterization data for the new compounds. CCDC 2100650. For ESI and crystallographic data in CIF or other electronic format see DOI: 10.1039/d1ra06533e

with the rigid ligand $H_2$sbdc with bi-carboxyl acid group to construct a stable 3D porous MOF, and the Tb-MOF with coordinative unsaturated Tb centers are able to sever as an efficient heterogeneous catalyst for the cyanosilylation of a series of aldehyde substrates.[25]

## Experimental section

### Materials and instrumentation

All the chemicals were purchased from commercial sources and used without any further purification. $^1$H-NMR spectra were recorded with BRUKER AVANCE III 500 NMR instrument ($CDCl_3$ solution) at 500 MHz. The single-crystal structure was tested on a D8 Venture SMART-CCD instrument with Mo-K$\alpha$ radiation designed by Bruker from Germany. X-ray powder diffraction (XRD) measurements were performed with Cu-K$\alpha$ radiation source ($\lambda = 0.15406$ nm) at 40 kV voltage and 25 mA current. IR spectra were performed on an IS50 FT-IR instrument. Thermogravimetric analysis was finished on a SDTQ600 thermogravimetric analysis instrument under $N_2$ condition. The content of C, H and N was analysed by vario EL III elemental analysis instrument designed by Elementar Company from Germany.

### Synthesis of Tb-MOF

0.3 mmol (0.091 g) $H_2$sbdc and 0.2 mmol (0.091 g) $Tb(NO_3)_3\cdot 6H_2O$ were mixed in a 9 mL bottle with 5 mL EtOH and 1 mL $H_2O$ stirring at room temperature for 3 h. Then sealed and placed in a pre-heated oven, and kept it at 140 °C for 4 days. The product was cooled to room temperature in 2 days. The crystals were formed under static conditions for 10 days. The resulting solid was filtered, washed with methanol and diethyl ether. Finally, the colorless block crystals were obtained and dried in vacuum at room temperature for one day (elemental analysis C: 37.31%; H: 2.679%).

### The method of catalysis by Tb-MOF

The typical experiment was performed as the following condition: substrate (0.5 mmol), trimethylsilyl cyanide (1.2 mmol), catalyst (12.79 mg, 4% mol of the substrate, based on the metal ions), and DCM (2 mL) in a 6 mL glass bottle in Ar environment at room temperature under continuously stirring. The corresponding yields of targeted products were successfully monitored by applying the NMR approach, which was added 0.5 mmol 1,3,5-trimethoxybenzene as an internal standard substance.

### Crystallography

X-ray intensities of the complexes were collected on a Bruker D8 Venture CCD diffractometer with graphite-monochromated Mo-K$\alpha$ ($\lambda = 0.71073$ Å) using the SMART and SAINT programs. The structures were solved by direct methods and refined on $F^2$ by full-matrix least-squares methods with SHELXTL-2018.

**Crystal data for Tb-MOF.** $[Tb_2(sbdc)_3(H_2O)_3]$, $M = 1278.63$, triclinic, space group $P\bar{1}$, colorless block, $a = 13.907$ (1) Å, $b = 14.243$ (1) Å, $c = 14.994$ (1) Å, $\alpha = 118.151$ (1), $\beta = 99.052$ (2), $\gamma = 103.126$ (2), $V = 2426.3$ (3) Å$^3$, $Z = 2$, $D_c = 1.750$ g cm$^{-3}$, $\mu$(Mo-K$\alpha$) = 0.71073 Å, $T = 296$ (2) K. 52 159 unique reflections [$R_{int} = 0.0603$], final $R_1$ [with $I > 2\sigma(I)$] = 0.0337, w$R_2$ (all data) = 0.0928, GOOF = 1.079. CCDC number: 2100650.†

In the structural refinement of Tb-MOF, except the partly occupied parts, the other non-hydrogen atoms were refined anisotropically and hydrogen atoms were fixed geometrically at calculated distances and allowed to ride on the parent non-hydrogen atoms. The highly disordered solvent molecules could not be located, and hence in the final refinement, the electron density was treated with the SQUEEZE routine in the PLATON program package.

## Results and discussion

Three-dimensional (3D) Tb-MOF was prepared using a rigid ligand 5,5-dioxo-5*H*-dibenzo[*b*,*d*]thiophene-3,7-dicarboxylic acid (namely $H_2$sbdc) and $Tb(NO_3)_3\cdot 6H_2O$ by using a solvothermal method to synthesize a novel material.[26] Tb-MOF can be considered as a highly efficient heterogeneous catalyst which was anticipated to catalyze the cyanosilylation of aldehyde based on its Lewis acid sites and porous structure.

The single crystal X-ray diffraction data showed that the obtained Tb-MOF crystallizes in $P\bar{1}$ space group (CCDC 2100650†). The asymmetric unit of Tb-MOF contained two Tb(III) ions, three $H_2$sbdc organic ligands, and three coordinated $H_2O$ molecules. As seen in Fig. 1a, Tb(1) and Tb(2) had two different coordination modes, of which coordinated numbers were both eight. Tb(1) was coordinated with eight oxygen atoms (Tb–O = 2.27–2.52 Å) from seven di-monodentate carboxyl groups in different ligands, and one water molecule. Tb(2) was coordinated with eight oxygen atoms (Tb–O = 2.26–2.53 Å) from four di-monodentate carboxyl groups in different ligands, one bi-dentate carboxyl group, and two water molecules, which was similar to some other works of Tb-MOFs reported before.[27] Tb(1) and Tb(2) were linked through two di-monodentate carboxyl groups and on $\mu_2$-oxygen atom of the

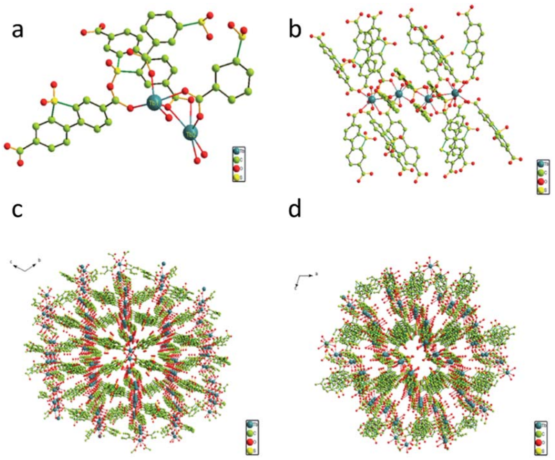

Fig. 1 (a) The asymmetric unit of Tb-MOF; (b) Tb4 units in Tb-MOF; (c) view of the 3D structure along *a* direction; (d) view of the 3D structure along *b* direction. Hydrogen atoms were omitted for clarity.

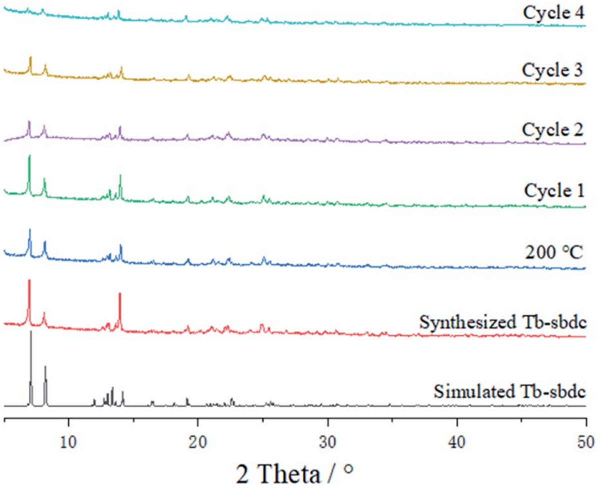

Fig. 2 The PXRD spectra. (black bar) Simulated Tb-MOF; (red bar) Tb-MOF; (blue bar) Tb-MOF Heated to 200 °C; (green bar) cycle one for catalysis of *m*-methoxybenzaldehyde; (purple bar) cycle two for catalysis of *m*-methoxybenzaldehyde; (yellow bar) cycle three for catalysis of *m*-methoxybenzaldehyde; (light blue bar) cycle four for catalysis of *m*-methoxybenzaldehyde.

didentate carboxy group. The two adjacent Tb(1) centers were bridged by four di-monodentate carboxyl groups, forming a paddle wheel dinuclear Tb(2) core by which the two Tb(1)–Tb(2) units were linked to form a zigzag tetra-nuclear unit. And the tetra-nuclear unit was further extended by the bi-carboxyl ligands, resulting in a 3D framework having channels along the *a* and *b* direction with the area of the pore was about 7.5 × 5.0 $Å^2$ and 9.0 × 5.5 $Å^2$ respectively, which were available for guest accommodation and exchange. The metal centers having removable water molecules were well-positioned in the channels. The results obviously demonstrated that Tb-MOF not only had lots of open metal Tb(III) sites but also contained lots of cavities as Lewis acids sites simultaneously, resulting in its potential applications in the catalytic field. The PXRD profile of the synthesized solid sample (Fig. 2) was carried out at ambient temperature and 200 °C, respectively. The characteristic diffraction lines of prepared Tb-MOF and Tb-MOF heated to 200 °C were similar with the simulated from the single crystal data of Tb-MOF, revealing the purity and stability of the product Tb-MOF.

Thermogravimetric analysis (TGA) demonstrated that in the range of 25–800 °C which increased 10 °C per minute in $N_2$ atmosphere. As obviously displayed in Fig. 3, the TGA result of the fresh synthesized Tb-MOF demonstrated a slow weight loss of 8% before 200 °C, corresponding to the loss of water and EtOH molecules. Tb-MOF became metal oxide and its structure collapsed when the temperature raised to 500 °C. It indicated that the framework of Tb-MOF was stable below 500 °C.

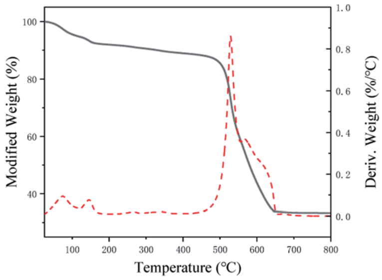

Fig. 3 The TGA spectra of Tb-MOF.

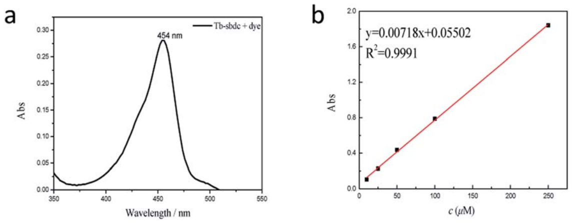

Fig. 4 (a) The UV-vis absorption spectra of released 2′,7′-dichlorofluorescein from Tb-MOF; (b) the concentration of 2′,7′-dichlorofluorescein was determined by comparing the UV-vis absorption with a standard curve.

After treating 10 mg Tb-MOF with 2′,7′-dichlorofluorescein in DCM for 24 h, the product was filtered and washed with DCM. Then HCl was used to destroy the structure of Tb-MOF so that the quantity of 2′,7′-dichlorofluorescein in the channels of Tb-MOF could be tested by UV-vis adsorption. The result in Fig. 4 showed that Tb-MOF can adsorb 6.3% 2′,7′-dichlorofluorescein of its weight, which could prove that Tb-MOF had enough pores and a good ability to adsorb small molecules.[28]

Since the addition of cyanide to a carbonyl compound to form a cyanohydrin was one of the fundamental C–C bond-forming reactions in organic chemistry and had frequently been at the forefront of advances in chemical transformations,[29] the catalytic ability of Tb-MOF for the cyanosilylation of the aromatic aldehyde was further studied in the detail due to the uniformly dispersed Lewis acid sites and the size of its pores in the whole structure.[30]

Therefore, *p*-methoxybenzaldehyde with TMSCN catalyzed by Tb-MOF was studied in different solutions. As we could see in Table 1, Tb-MOF had no catalytic ability in EtOH for this reaction, even the mixture was stirred for 12 h. And the yield of the reaction in MeOH was much lower than those in DCM, THF, and $CH_3CN$. Considering the stability of the MOF catalyst and the separation of the product, DCM was chosen as the solvent of the reaction for further study. Consequently, the reaction condition was optimized as the addition of 2.4 equivalent of TMSCN (Fig. S63†) and 12 h (Fig. S64†) under Ar at room temperature.

Table 1 The yields in different solutions (0.5 mmol *p*-methoxybenzaldehyde, 1.2 mmol TMSCN, 4 mol% Tb-MOF, in 2 mL solution, under Ar condition)

| Entry | Solvent | Conv. (%) |
|---|---|---|
| 1 | MeCN | 85 |
| 2 | THE | 82 |
| 3 | DCM | 78 |
| 4 | MeOH | 14 |
| 5 | EtOH | 0 |

Therefore, different aromatic aldehydes, which had different electronic effect, spatial effect, and fatty aldehyde were selected. Table 2 showed the results based on 12 different aldehyde substrates and trimethylsilyl cyanide in the presence of Tb-MOF. Most of them had a higher yield. Even, the yield of 1-naphthalene formaldehyde reached 77%. Table 3 showed the catalytic cyanosilylation of *o*-, *m*- and *p*-methoxybenzaldehyde in different conditions. The final yield of 3-methoxybenzaldehyde and 4-methoxybenzaldehyde were 85% and 81% after reacting 12 h. The reaction was monitored after reacting 4 h. The yield of *o*-, *m*-, and *p*-methoxybenzaldehyde was 28%, 30%, and 41%, respectively. The corresponding initial TOF was about 1.8 $h^{-1}$, 1.9 $h^{-1}$, and 2.6 $h^{-1}$, respectively. The catalyst Tb-MOF was filtered after reacting 4 h and let the reaction continue. The yield of 4-methoxybenzaldehyde increased a little to 47% after reacting 12 h, of which the catalyst Tb-MOF was removed after reacting 4 h. The yield of this reaction was 0 without any catalyst for 12 h. The yield of the reaction catalyzed by the ligand without Tb-MOF was 0 either. The yield had no significant change when the catalyst was doubled. These consequences demonstrated that the ligand couldn't catalyze this reaction and Tb-MOF was necessary for this reaction. The Lewis acid sites in the channel of Tb-MOF could activate the substrates, which could make the reaction continue. Furthermore, as the yields of *o*-, *m*- and *p*-methoxybenzaldehyde after 12 h are 82%, 79%, 78%, catalyst Tb-MOF had no prominent electronic effect on this reaction. However, the yield of *p*-benzyloxybenzaldehyde and 4-(diethylamino)salicylaldehyde were 66% and 57%, which were lower than other substrates. It seemed that the substrates which had larger sizes didn't fit the pores of Tb-MOF well, indicating that the activation of substrates should be occurred in the pores of Tb-MOF. Table 2 also showed that all the TON of the 12 product were about 20, which were not at a high level. Consequently, 5 mmol *p*-methoxybenzaldehyde, 12 mmol TMSCN, and 0.2% mmol Tb-MOF with no solvent were stirred at room temperature under Ar condition. Notably, the yield of solvent free condition was about 92%, and the TON could reach about 460 with the MOF catalyst being 0.2 mol%, which demonstrated that Tb-MOF had a good ability of catalyzing cyanosilylation. The results above demonstrated that the Tb-MOF had a good ability for catalyzing most kinds of aldehydes for higher yields as a heterogeneous catalyst.

Table 2 Catalytic cyanosilylation of different substrates in the presence of Tb-MOF. Reaction conditions: $(CH_3)_3SiCN$: 1.2 mmol, aldehyde: 0.5 mmol, Tb-MOF catalysts (4 mol%), room temperature under Ar for 12 h

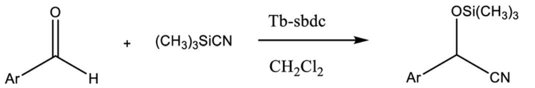

| Entry | Substrate | Product | Conversion (%) | TON |
|---|---|---|---|---|
| 1 | 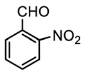 | 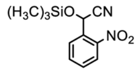 | 78 | 20 |
| 2 | 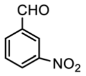 | 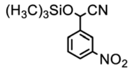 | 85 | 21 |
| 3 | 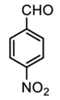 | 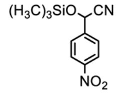 | 81 | 20 |
| 4 | 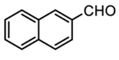 | 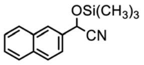 | 77 | 19 |
| 5 | 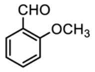 | 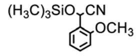 | 82 | 21 |
| 6 | 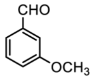 | 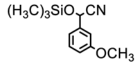 | 79 | 20 |
| 7 | 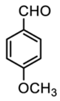 | 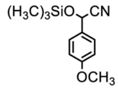 | 78 | 20 |
| 8 |  | 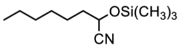 | 74 | 19 |
| 9 | 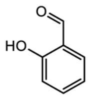 | 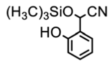 | 85 | 21 |
| 10 | 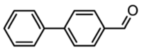 | 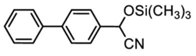 | 83 | 21 |
| 11 | 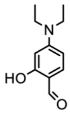 | 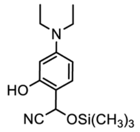 | 57 | 14 |
| 12 | 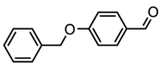 | 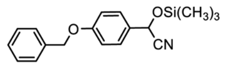 | 66 | 17 |
| 13[a] | 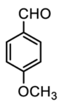 | 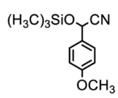 | 92 | 460 |

[a] 5 mmol *p*-methoxybenzaldehyde, 12 mmo1 TMSCN, and 0 2% mmol Tb-MOF with no solvent were stirred at room temperature under Ar condition.

To test the recyclability of the catalyst Tb-MOF, four cycles of cyanosilylation reaction in DCM were performed. Tb-MOF was separated by filtration from the reaction mixture after 12 hours, washed with DCM, dried under vacuum overnight, and reused in the next reaction run. The second, the third, and the forth cycles were completed under the same condition as the first cycle. From the PXRD measurements of the recovered catalyst in Fig. 2, Tb-MOF retained its structural framework even after three cycling reaction process. However, the decrease of the PXRD could be found in the forth cycle. As shown in Fig. 5, reactions catalyzed by Tb-MOF showed a slight decrease after three cycles, which demonstrated that the heterogeneous Tb-MOF had a better advantage than the homogeneous catalyst. In the forth cycle, the yields decreased more than the first three cycles, which fitted the PXRD results. TON of *o*-, *m*-, and *p*-methoxybenzaldehyde for all the four cycles were 80, 74, and 69, respectively. As a result, Tb-MOF had a good ability for

Table 3 Catalytic cyanosilylation *o*-, *m*- and *p*-methoxybenzaldehyde in different conditions

| Substrate | 12 h | 4 h | 4–12 h | Double catalyst | Without catalyst | Ligand |
|---|---|---|---|---|---|---|
| 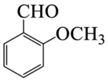 CHO OCH$_3$ | 82 | 28 | 46 | 81 | 0 | 0 |
| 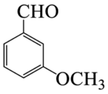 CHO OCH$_3$ | 79 | 30 | 43 | 83 | 0 | 0 |
| 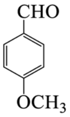 CHO OCH$_3$ | 78 | 41 | 47 | 80 | 0 | 0 |

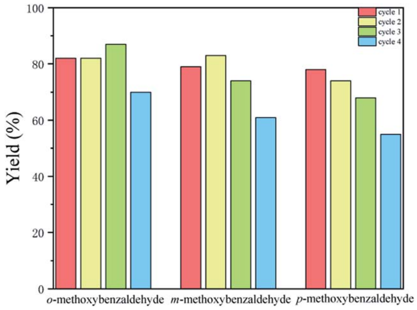

Fig. 5 The yields for three cycles (0.5 mmol *p*-methoxybenzaldehyde, 1.2 mmol TMSCN, 0.01 mmol Tb-MOF, in 2 mL DCM at room temperature under Ar condition).

recyclable catalyzing cyanosilylation for at least three times without the yields' going down.

To test whether Tb-MOF could adsorb the substrate, 0.01 mmol Tb-MOF, 3 mmol substrate with 2 mL DCM in a 6 mL glass bottle were under continuously stirring for 24 h. Then the solid was filtered, washed by DCM and dried in vacuum. Fig. 6 was the IR spectrogram, which showed the differences between Tb-MOF and Tb-MOF with the substrate inside. The peak of the C═O bond of 2-naphthaldehyde was 1701 cm$^{-1}$, while the peak moved to 1710 after 2-naphthaldehyde was treated with Tb-MOF. It demonstrated that the substrate could be absorbed by the pores of Tb-MOF and had interaction with Tb-MOF.

To test the ability for activating the substrates of Tb-MOF, 2 mg Tb-MOF with 2-naphthaldehyde from 0 to 0.001 M was treated. A significant quenching of the fluorescence intensity could be seen in Fig. 7. It was important to note that the sorption of 2-naphthaldehyde caused the luminescence quenching. The value of $I_0/I$ and the concentration exhibited a linear relationship at a lower concentration range (0–0.5 mM), which fitted the Stern–Volmer (SV) equation, $I_0/I = K\text{sv}[\text{M}] + 1$ (where $I_0$ represented the initial intensity of the peak at 615 nm, $I$ represented the intensity at different concentrations of 2-naphthaldehyde suspension, [M] represented the concentration of 2-naphthaldehyde, and $K$sv represented the quenching constant (M$^{-1}$)), with a correlation coefficient ($R^2$) of 0.98.[31] The $K_{\text{SV}}$ value for 2-naphthaldehyde was counted to be 1.26 × 10$^3$ M$^{-1}$.[32] The high $K_{\text{SV}}$ allowed us to easily identify the existence of a small amount of aldehyde in solution. As previously mentioned, the relationship between $I_0/I$ and the concentration of substrate could be well fitted into the SV equation at lower concentrations, suggesting the interaction with quenching substrates, forming complexes and influencing the luminescence spectra of luminescent substances.[33] The fluorescence titration proved that the catalysis of the reaction was in the channel of Tb-MOF,

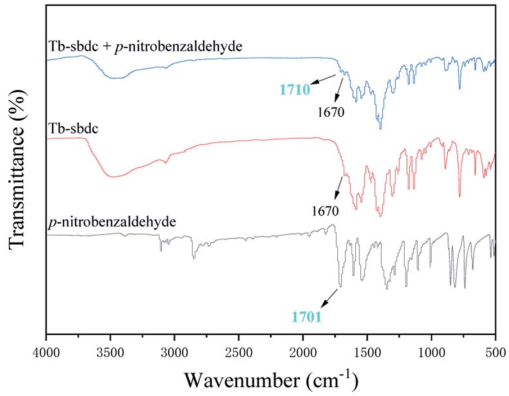

Fig. 6 The IR spectra of Tb-MOF with different *p*-nitrobenzaldehyde.

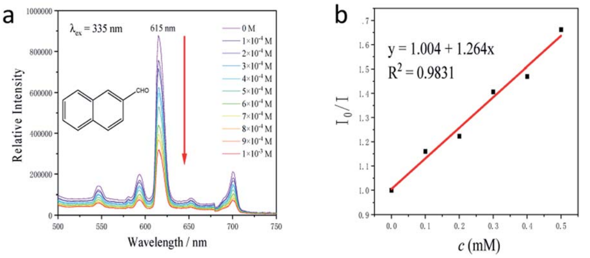

Fig. 7 (a)Luminescent spectra of Tb-MOF emulsion in DCM upon addition of substrates up to 0.001 M (excited at 335 nm). (b) The plot of $I_0/I$ *vs.* the lower concentration (0–0.5 mM) of 2-naphthaldehyde which showed intensities at 615 nm as a function of substrates (excited at 335 nm).

which could also recognize the substrates. The Lewis-acid sites played a dormant role in the cyanosilylation. In this case, the luminescence behavior of Tb-MOF suggested the sorption of the substrate into the MOFs and the possible interaction between the aldehyde substrate and the Tb centers. Based on the experimental results above and the works reported before, a possible reaction mechanism was presented to explain the reaction process of cyanosilylation catalyzed by Tb-MOF: the substrates were activated by the coordinatively unsaturated Tb centres to react with TMSCN, which was shown in Fig. S65.† The products were removed by other substrates, meanwhile, Tb-MOF continued to activate the substrates in the next catalytic turn.[34]

## Conclusions

In conclusion, a novel Tb(III)-based metal–organic framework was successfully synthesized, which could be considered as an efficient heterogeneous catalyst for the cyanosilylation of different aldehydes at room temperature because of its pores and the activation ability for the substrates of its Lewis acid sites. Meanwhile, Tb-MOF exhibited a high TON (TON = 460) in solvent free condition and a good recyclability for these reactions in solvent condition at least three times. Compared to other transition metal organic frameworks,[24] which were designed for catalyzing cyanosilylation in solvent free condition, Tb-MOF had a higher TON. As a result, Tb-MOF was considered as a good heterogeneous catalyst for cyanosilylation and had a good prospect for further study. We hope that this work can offer a useful and meaningful method to use such ligands to synthesize MOFs for sensing or absorbing organic molecules towards environmental and catalyzing different reactions.

## Conflicts of interest

There are no conflicts to declare.

## Acknowledgements

We gratefully acknowledge financial support from the National Natural Science Foundation of China (U1608224).

## Notes and references

1 (*a*) H. Raza, *et al.*, Synthesis of a 2D copper(II)-carboxylate framework having ultrafast adsorption of organic dyes, *J. Colloid Interface Sci.*, 2021, **602**, 43–54; (*b*) Q. F. Lin, *et al.*, Three 3D Lanthanide coordination polymers: Synthesis, luminescence and magnetic properties, *J. Mol. Struct.*, 2021, **1234**, 130167; (*c*) J. Wang, *et al.*, Two 3D supramolecular isomeric Zn(II)-MOFs as photocatalysts for photodegradation of methyl violet dye, *Dyes Pigm.*, 2021, **190**, 109285; (*d*) J. D. Yi, *et al.*, Conductive Two-Dimensional Phthalocyanine-based Metal–Organic Framework Nanosheets for Efficient Electroreduction of $CO_2$, *Angew. Chem., Int. Ed.*, 2021, **60**, 2–9; (*e*) Y. Liu, *et al.*, The Synthesis of Hexaazatrinaphthylene-Based 2D Conjugated Copper Metal-Organic Framework for Highly Selective and Stable Electroreduction of $CO_2$ to Methane, *Angew. Chem., Int. Ed.*, 2021, **60**, 1–8; (*f*) Y. H. Luo, *et al.*, 2D hydrogen-bonded organic frameworks: in-site generation and subsequent exfoliation, *Chem. Commun.*, 2021, **57**, 5901–5904; (*g*) Q. Bi, *et al.*, Hierarchical core-shell 2D MOF nanosheet hybrid arrays for high-performance hybrid supercapacitors, *Dalton Trans.*, 2021, **50**, 8179–8188.

2 (*a*) X. Ren, *et al.*, Diversified strategies based on nanoscale metal-organic frameworks for cancer therapy: The leap from monofunctional to versatile, *Coord. Chem. Rev.*, 2021, **431**, 213676; (*b*) L. Fan, *et al.*, A Series of Metal-Organic Framework Isomers Based on Pyridinedicarboxylate Ligands: Diversified Selective Gas Adsorption and the Positional Effect of Methyl Functionality, *Inorg. Chem.*, 2021, **60**, 2704–2715; (*c*) M. A. Gordillo, *et al.*, The Advent of Electrically Conducting Double-Helical Metal-Organic Frameworks Featuring Butterfly-Shaped Electron-Rich π-Extended Tetrathiafulvalene Ligands, *ACS Appl. Mater. Interfaces*, 2020, **12**, 12955–12961; (*d*) D. Sun, *et al.*, From Mixed-Metal MOFs to Carbon-Coated Core-Shell Metal Alloy@Metal Oxide Solid Solutions: Transformation of Co/Ni-MOF-74 to $Co_xNi_{1-x}$@$Co_yNi_{1-y}$O@C for the Oxygen Evolution Reaction, *Inorg. Chem.*, 2017, **56**, 5203–5209; (*e*) Y. F. Niu, *et al.*, Solvent-mediated secondary building units (SBUs) diversification in a series of $Mn^{II}$-based metal-organic frameworks (MOFs), *J. Solid State Chem.*, 2016, **241**, 18–25.

3 (*a*) J. Kim, *et al.*, Enhancement of hydrogen storage capacity and hydrostability of metal-organic frameworks (MOFs) with surface-loaded platinum nanoparticles and carbon black, *Microporous Mesoporous Mater.*, 2015, **202**, 8–15; (*b*) J. L. C. Rowsell and O. M. Yaghi, Metal–organic frameworks: a new class of porous materials, *Microporous Mesoporous Mater.*, 2004, **73**, 3–14.

4 (*a*) D. Ursueguía, *et al.*, Metal-Organic Frameworks (MOFs) as methane adsorbents: From storage to diluted coal mining streams concentration, *Sci. Total Environ.*, 2021, **790**, 148211; (*b*) P. A. S. Vavazos, *et al.*, Fluorinated MIL-101 for carbon capture utilization and storage: uptake and diffusion studies under relevant industrial conditions, *RSC Adv.*, 2021, **11**, 13304–13310; (*c*) C. Altintas, *et al.*, Machine Learning Meets with Metal Organic Frameworks for Gas Storage and Separation, *J. Chem. Inf. Model.*, 2021, **61**, 2131–2146; (*d*) F. E. Chen, *et al.*, Biocompatible metal–organic frameworks for the storage and therapeutic delivery of hydrogen sulfide, *Chem. Sci.*, 2021, **12**, 7848–7857; (*e*) S. Lin, *et al.*, An Isomeric Copper-Diisophthalate Framework Platform for Storage and Purification of $C_2H_2$ and Exploration of the Positional Effect of the Methyl Group, *Eur. J. Inorg. Chem.*, 2021, 2070–2077.

5 (*a*) J. X. Liu, *et al.*, 3.Al-Based Metal-Organic Framework MFM-300 and MIL-160 for $SO_2$ Capture: A Molecular Simulation Study, *Fluid Phase Equilib.*, 2021, **536**, 112963; (*b*) X. Dong, *et al.*, Recycling Plastic Waste for Environmental Remediation in Water Purification and $CO_2$

Capture, *ACS Appl. Polym. Mater.*, 2020, **2**, 2586–2593; (*c*) Z. Hu, *et al.*, $CO_2$ Capture in Metal-Organic Framework Adsorbents: An Engineering Perspective, *Adv. Sustainable Syst.*, 2019, **3**, 1800080; (*d*) L. A. Darunte, *et al.*, Moving Beyond Adsorption Capacity in Design of Adsorbents for $CO_2$ Capture from Ultradilute Feeds: Kinetics of $CO_2$ Adsorption in Materials with Stepped Isotherms, *Ind. Eng. Chem. Res.*, 2019, **58**, 366–377.

6 (*a*) Y. Zeng, *et al.*, Molecular simulations for adsorption and separation of thiophene and benzene in Cu-BTC and IRMOF-1 metal–organic frameworks, *Sep. Purif. Technol.*, 2012, **95**, 149–156; (*b*) X. Han, *et al.*, Fine-tuning the pore structure of metal–organic frameworks by linker substitution for enhanced hydrogen storage and gas separation, *CrystEngComm*, 2021, **23**, 3026–3032; (*c*) X. P. Fu, *et al.*, Metal-organic frameworks for $C_2H_2/CO_2$ separation, *Dalton Trans.*, 2020, **49**, 16598–16607; (*d*) Z. Ju, *et al.*, Dynamic metal-organic frameworks for the separation of hydrogen isotopes, *Dalton Trans.*, 2020, **49**, 16617–16622; (*e*) Y. Zhao, *et al.*, Design of thin and tubular MOFs-polymer mixed matrix membranes for highly selective separation of $H_2$ and $CO_2$, *Sep. Purif. Technol.*, 2019, **220**, 197–205; (*f*) S. Yang, *et al.*, Elucidating Charge Separation Dynamics in a Hybrid Metal-Organic Framework Photocatalyst for Light-Driven $H_2$ Evolution, *J. Phys. Chem. C*, 2018, **122**, 3305–3311.

7 (*a*) Y. B. N. Tran, *et al.*, Series of M-MOF-184 (M = Mg, Co, Ni, Zn, Cu, Fe) Metal-Organic Frameworks for Catalysis Cycloaddition of $CO_2$, *Inorg. Chem.*, 2020, **59**, 16747–16759; (*b*) U. Patel, *et al.*, Zn(II)/Cd(II)-Based Metal-Organic Frameworks as Bifunctional Materials for Dye Scavenging and Catalysis of Fructose/Glucose to 5-Hydroxymethylfurfural, *Inorg. Chem.*, 2021, **60**, 9181–9191; (*c*) R. R. Tuttle, Copper Metal-Organic Framework Surface Catalysis: Catalyst Poisoning, IR Spectroscopic, and Kinetic Evidence Addressing the Nature and Number of the Catalytically Active Sites En Route to Improved Applications, *ACS Appl. Mater. Interfaces*, 2020, **12**, 39043–39055; (*d*) Y. Gao, *et al.*, In Situ Synthesis of Defect-Engineered MOFs as a Photoregenerable Catalytic Adsorbent: Understanding the Effect of LML, Adsorption Behavior, and Photoreaction Process, *ACS Appl. Mater. Interfaces*, 2020, **12**, 12706–12716; (*e*) J. N. Hall and P. Bollini, Metal-Organic Framework MIL-100 Catalyzed Acetalization of Benzaldehyde with Methanol: Lewis or Brønsted Acid Catalysis?, *ACS Catal.*, 2020, **10**, 3750–3763; (*f*) C. Wang, *et al.*, Metal-Organic Frameworks in Solid-Gas Phase Catalysis, *ACS Catal.*, 2019, **9**, 130–146; (*g*) L. Yang, *et al.*, A Versatile Porous Silver-Coordinated Material for the Heterogeneous Catalysis of Chemical Conversion with Propargylic Alcohols and $CO_2$, *Nanomaterials*, 2019, 1566.

8 (*a*) Y. Shi, *et al.*, A novel terbium metaleorganic framework for luminescence sensing of pyridine: Synthesis, structure, selectivity, sensitivity and recyclability, *J. Rare Earths*, 2020, **38**, 1231–1236; (*b*) G. E. Gomez and F. Ronocaroli, Photofunctional metal-organic framework thin films for sensing, catalysis and device fabrication, *Inorg. Chim. Acta*, 2020, **513**, 119926; (*c*) É. Whenlan, *et al.*, Tuning photoactive metal–organic frameworks for luminescence and photocatalytic applications, *Coord. Chem. Rev.*, 2021, **437**, 213757.

9 (*a*) S. Pandey, *et al.*, Electronic structures and magnetism of Zr-, Th-, and U-based metal-organic frameworks (MOFs) by density functional theory, *Comput. Mater. Sci.*, 2020, **184**, 109903; (*b*) M. N. Ahamad, *et al.*, Cu(II) MOFs Based on Bipyridyls: Topology, Magnetism, and Exploring Sensing Ability toward Multiple Nitroaromatic Explosives, *ACS Omega*, 2019, **4**, 7738–7749; (*c*) K. Iman, *et al.*, Topology, magnetism and dye adsorption properties of metal organic frameworks (MOFs) synthesized from bench chemicals, *CrystEngComm*, 2019, **21**, 5299–5309; (*d*) C. Qiao etal, Pore-size-tuned host–guest interactions in Co-MOFs *via* in situ microcalorimetry: adsorption and magnetism, *J. Mater. Chem. C*, 2017, **5**, 1064–1073; (*e*) S. I. Vasylevs'kyy, *et al.*, 1,2,4-Triazolyl-Carboxylate-Based MOFs Incorporating Triangular Cu(II)-Hydroxo Clusters: Topological Metamorphosis and Magnetism, *Inorg. Chem.*, 2014, **53**, 3642–3654; (*f*) N. Zhang, *et al.*, Solvent-controlled structural diversity observed in three Cu(II) MOFs with a 2,2'-dinitro-biphenyl-4,4'-dicarboxylate ligand: synthesis, structures and magnetism, *RSC Adv.*, 2015, **5**, 70772–70780.

10 (*a*) M. Abedi, *et al.*, Hierarchical mesoporous zinc-imidazole dicarboxylic acid MOFs: Surfactant-directed synthesis, pH-responsive degradation, and drug delivery, *Int. J. Pharm.*, 2021, **602**, 120685; (*b*) A. Ringaci, *et al.*, Metal-organic frameworks for simultaneous gene and small molecule delivery *in vitro* and *in vivo*, *Chem. Eng. J.*, 2021, **418**, 129386; (*c*) M. N. Hasan, *et al.*, Sensitization of nontoxic MOF for their potential drug delivery application against microbial infection, *Inorg. Chim. Acta*, 2021, **523**, 120381; (*d*) S. Sharma, *et al.*, Copper-Gallic Acid Nanoscale Metal-Organic Framework for Combined Drug Delivery and Photodynamic Therapy, *ACS Appl. Bio Mater.*, 2019, **2**, 2092–2101; (*e*) Y. Li, *et al.*, MOF nanoparticles with encapsulated dihydroartemisinin as a controlled drug delivery system for enhanced cancer therapy and mechanism analysis, *J. Mater. Chem. B*, 2020, **8**, 7382–7389; (*f*) J. Zhao, *et al.*, Development of a Tau-Targeted Drug Delivery System Using a Multifunctional Nanoscale Metal-Organic Framework for Alzheimer's Disease Therapy, *ACS Appl. Mater. Interfaces*, 2020, **12**, 44447–44458.

11 (*a*) Q. Tang, *et al.*, Color Tuning and White Light Emission *via* in Situ Doping of Luminescent Lanthanide Metal-Organic Frameworks, *Inorg. Chem.*, 2014, **53**, 289–293; (*b*) Q. Yao, *et al.*, Series of Highly Stable Isoreticular Lanthanide Metal-Organic Frameworks with Expanding Pore Size and Tunable Luminescent Properties, *Chem. Mater.*, 2015, **27**, 5332–5339.

12 (*a*) R. M. Cedeno, *et al.*, Bandgap Modulation in Zr-Based Metal-Organic Frameworks by Mixed-Linker Approach, *Inorg. Chem.*, 2021, **60**, 8908–8916; (*b*) É. Whelan, *et al.*, Tuning photoactive metal-organic frameworks for luminescence and photocatalytic applications, *Coord. Chem. Rev.*, 2021, **437**, 213757.

13 (*a*) M. K. Matikolaei and E. Binaeian, Boosting Ammonia Uptake within Metal-Organic Frameworks by Anion Modulating Strategy, *ACS Appl. Mater. Interfaces*, 2021, **13**, 27159–27168; (*b*) S. E. Ashbrook, *et al.*, $^{17}$O NMR spectroscopy of crystalline microporous materials, *Chem. Sci.*, 2021, **12**, 5016–5036.

14 K. Y. A. Lin and F. K. Hsu, Magnetic iron/carbon nanorods derived from a metal organic framework as an efficient heterogeneous catalyst for the chemical oxidation process in water, *RSC Adv.*, 2015, **5**, 50790–50800.

15 (*a*) Q. G. Zhai, *et al.*, Design of Pore Size and Functionality in Pillar-Layered Zn-TriazolateDicarboxylate Frameworks and Their High $CO_2/CH_4$ and C2 Hydrocarbons/$CH_4$ Selectivity, *Inorg. Chem.*, 2015, **54**, 9862–9868; (*b*) T. He, *et al.*, Competitive Coordination Strategy to Finely Tune Pore Environment of Zirconium-Based Metal-Organic Frameworks, *ACS Appl. Mater. Interfaces*, 2017, **9**, 22732–22738; (*c*) S. A. A. Razavi, *et al.*, Improvement of Methane-Framework Interaction by Controlling Pore Size and Functionality of Pillared MOFs, *Inorg. Chem.*, 2017, **56**, 2581–2588.

16 (*a*) K. Roztoki, *et al.*, Combining *In Situ* Techniques (XRD, IR, and $^{13}$C NMR) and Gas Adsorption Measurements Reveals $CO_2$-Induced Structural Transitions and High $CO_2/CH_4$ Selectivity for a Flexible Metal-Organic Framework JUK-8, *ACS Appl. Mater. Interfaces*, 2021, **13**, 28503–28513; (*b*) A. Schlachter, *et al.*, Porphyrin-Containing MOFs and COFs as Heterogeneous Photosensitizers for Singlet Oxygen-Based Antimicrobial Nanodevices, *ACS Appl. Mater. Interfaces*, 2021, **13**, 26651–26672; (*c*) C. Yue, *et al.*, Study on the Stability, Evolution of Physicochemical Properties, and Postsynthesis of Metal-Organic Frameworks in Bubbled Aqueous Ozone Solution, *ACS Appl. Mater. Interfaces*, 2021, **13**, 26264–26277.

17 Y. Takashima, *et al.*, In Situ Generation and Immobilization of an Activated Rh Complex Catalyst in a Metal-Organic Framework for Hydrogenation at Low $H_2$ Pressure, *Eur. J. Inorg. Chem.*, 2017, 5344–5349.

18 (*a*) W. Cao, *et al.*, Lanthanide metal-organic frameworks with nitrogen functional sites for the highly selective and sensitive detection of NADPH, *Chem. Commun.*, 2020, **56**, 10851–10854; (*b*) H. Y. Li, *et al.*, Functional metal-organic frameworks as effective sensors of gases and volatile compounds, *Chem. Soc. Rev.*, 2020, **4**, 6364–6401.

19 (*a*) Y. Liu, *et al.*, Porous and Robust Lanthanide Metal-Organoboron Frameworks as Water Tolerant Lewis Acid Catalysts, *Inorg. Chem.*, 2013, **52**, 10286–10291; (*b*) C. Pagis, *et al.*, Lanthanide-Based Metal Organic Frameworks: Synthetic Strategies and Catalytic Applications, *ACS Catal.*, 2016, **6**, 6063–6072; (*c*) A. Bavykina, *et al.*, Metal-Organic Frameworks in Heterogeneous Catalysis: Recent Progress, New Trends, and Future Perspectives, *Chem. Rev.*, 2020, **120**, 8468–8535.

20 (*a*) Z. Li, *et al.*, Aperture-Opening Encapsulation of a Transition Metal Catalyst in a Metal-Organic Framework for $CO_2$ Hydrogenation, *J. Am. Chem. Soc.*, 2018, **140**, 8082–8085; (*b*) Y. Chen, *et al.*, Aluminum metal-organic framework as a new host for preparation of encapsulated metal complex catalysts, *Catal. Commun.*, 2015, **64**, 91–95.

21 G. Chen, *et al.*, Fluorescence and electrochemical assay for bimodal detection of lead ions based on Metal–Organic framework nanosheets, *Talanta*, 2021, **232**, 122405.

22 G. K. S. Prakash, H. Vaghoo, C. Panja, V. Surampudi, R. Kultyshev, T. Mathew and G. A. Olah, Effect of carbonates/phosphates as nucleophilic catalysts in dimethylformamide for efficient cyanosilylation of aldehydes and ketones, *Proc. Natl. Acad. Sci. U. S. A.*, 2007, **104**(9), 3026.

23 M. North, D. L. Usanov and C. Young, Lewis Acid Catalyzed Asymmetric Cyanohydrin Synthesis, *Chem. Rev.*, 2008, **108**, 5146.

24 Z. Zhang, J. Chen, Z. Bao, G. Chang, H. Xing and Q. Ren, Insight into the catalytic properties and applications of metal–organic frameworks in the cyanosilylation of aldehydes, *RSC Adv.*, 2015, **5**, 79355–79360.

25 (*a*) W. Xu, *et al.*, A Robust $Tb^{III}$-MOF for Ultrasensitive Detection of Trinitrophenol: Matched Channel Dimensions and Strong Host-Guest Interactions, *Inorg. Chem.*, 2019, **58**, 8198–8207; (*b*) P. Wu, *et al.*, Lanthanide-Based Metal-Organic Frameworks Containing "V-Shaped" Tetracarboxylate Ligands: Synthesis, Crystal Structures, "Naked-Eye" Luminescent Detection, and Catalytic Properties, *Inorg. Chem.*, 2020, **59**, 264–273; (*c*) Y. Zhang, *et al.*, Robust Bifunctional Lanthanide Cluster Based Metal-Organic Frameworks (MOFs) for Tandem Deacetalization-Knoevenagel Reaction, *Inorg. Chem.*, 2018, **57**, 2193–2198.

26 (*a*) E. Neofotistou, *et al.*, Unprecedented Sulfone-Functionalized Metal-Organic Frameworks and Gas-Sorption Properties, *Chem.–Eur. J.*, 2009, **15**, 4523–4527; (*b*) K. Kanaizuka, *et al.*, Design and Characterization of a Polarized Coordination Polymer of a Zinc(II) Biphenyldicarboxylate Bearing a Sulfone Group, *Chem. Lett.*, 2010, **39**, 2829.

27 H. M. Chai, *et al.*, A Multifunctional Tb-MOF Detector for $H_2O_2$, $Fe^{3+}$, $Cr_2O_7{}^{2-}$, and TPA Explosive Featuring Coexistence of Binuclear and Tetranuclear Clusters, *ACS Omega*, 2020, **5**, 33039–33046.

28 (*a*) X. Zhao, *et al.*, The application of MOFs-based materials for antibacterials adsorption, *Coord. Chem. Rev.*, 2021, **440**, 213970; (*b*) P. Brandt, *et al.*, Zirconium and Aluminum MOFs for Low-Pressure $SO_2$ Adsorption and Potential Separation: Elucidating the Effect of Small Pores and $NH_2$ Groups, *ACS Appl. Mater. Interfaces*, 2021, **13**, 29137–29149.

29 (*a*) D. Dang, P. Wu, C. He, Z. Xie and C. Duan, *J. Am. Chem. Soc.*, 2010, **132**, 14321; (*b*) M. North, D. L. Usanov and C. Young, *Chem. Rev.*, 2008, **108**, 5146.

30 (*a*) P. Y. Wu, *et al.*, Luminescent Sensing and Catalytic Performances of a Multifunctional Lanthanide-Organic Framework Comprising a Triphenylamine Moiety, *Adv. Funct. Mater.*, 2011, **21**, 2788–2794; (*b*) S. Horike, *et al.*, Size-Selective Lewis Acid Catalysis in a Microporous Metal-Organic Framework with Exposed $Mn^{2+}$ Coordination Sites, *J. Am. Chem. Soc.*, 2008, **130**, 5854–5855; (*c*) L. M. Aguirre-

Diaz, *et al.*, Toward understanding the structure-catalyst activity relationship of new indium MOFs as catalysts for solvent-free ketone cyanosilylation, *RSC Adv.*, 2015, **5**, 7058–7065.

31 Z. Yao, G. Li, J. Xu, T. Hu and X. Bu, A Water-Stable Luminescent Zn(II) Metal-Organic Framework as Chemosensor for High-Efficiency Detection of Cr(VI)-Anions (Cr2O72- and CrO42-) in Aqueous Solution, *Chem.–Eur. J.*, 2018, **24**, 3192–3198.

32 (*a*) Z. Hu, *et al.*, Effective detection of mycotoxins by a highly luminescent metal-organic framework, *J. Am. Chem. Soc.*, 2015, **137**, 16209–16215; (*b*) N. D. Rudd, *et al.*, Highly Efficient Luminescent Metal-Organic Framework for the Simultaneous Detection and Removal of Heavy Metals from Water, *ACS Appl. Mater. Interfaces*, 2016, **8**, 30294–30303; (*c*) H. Xu, *et al.*, Metalorganic framework nanosheets for fast response and highly sensitive luminescent sensing of Fe3+, *J. Mater. Chem. A*, 2016, **4**, 10900–10905.

33 (*a*) S. Zhu and B. Yan, A novel sensitive fluorescent probe of $S_2O_8^{2-}$and $Fe^{3+}$ based on covalent post-functionalization of a zirconium(IV) metal-organic framework, *Dalton Trans.*, 2018, **47**, 11586–11592; (*b*) J. Dong, *et al.*, Metal-Organic Frameworks with Tb4 Clusters as Nodes: Luminescent Detection of Chromium(VI) and Chemical Fixation of $CO_2$, *Inorg. Chem.*, 2017, **56**, 6244–6250; (*c*) R. Goswami, *et al.*, Guest-Induced Ultrasensitive Detection of Multiple Toxic Organics and $Fe^{3+}$ Ions in a Strategically Designed and Regenerative Smart Fluorescent Metal-Organic Framework, *ACS Appl. Mater. Interfaces*, 2019, **11**, 9042–9053; (*d*) C. Gogoi, M. Yousufuddin and S. Biswas, A new 3D luminescent Zn(II)-organic framework containing a quinoline-2,6-dicarboxylate linker for the highly selective sensing of Fe(III) ions, *Dalton Trans.*, 2019, **48**, 1766–1773.

34 (*a*) G. Kumar and R. Gupta, *Inorg. Chem.*, 2013, **52**, 10773; (*b*) J. A. Seckar and J. S. Thayer, *Inorg. Chem.*, 1976, **15**, 501.